SEISMICA

Potential Volcanic Origin of the 2023 Short-period Tsunami in the Izu Islands, Japan

A. Mizutani (iD) *[1,2], **D. Melgar** (iD) [2]

[1]Faculty of Science, Hokkaido University, Sapporo, Japan, [2]Department of Earth Sciences, University of Oregon, Eugene, U.S.A

Author contributions: *Conceptualization*: A. Mizutani. *Data Curation*: A. Mizutani. *Formal Analysis*: A. Mizutani. *Funding Acquisition*: A. Mizutani. *Investigation*: A. Mizutani. *Methodology*: A. Mizutani. *Project Administration*: A. Mizutani, D. Melgar. *Resources*: D. Melgar. *Software*: A. Mizutani. *Supervision*: D. Melgar. *Validation*: A. Mizutani. *Visualization*: A. Mizutani. *Writing – original draft*: A. Mizutani. *Writing – review & editing*: A. Mizutani, D. Melgar.

Abstract   On October 8, 2023, at 21:40 UTC (6:40 on October 9 local time), a tsunami warning was issued for the Izu Islands and southwest Japan. This tsunami was initially considered to be associated with the M_w 4.7 earthquake at 20:25 UTC (5:25 JST). However, we know events of this magnitude are far too small to generate observed tsunamis from coseismic deformation alone. In this study, we analyzed the ocean-bottom pressure records of DONET and S-net, real-time cabled observation networks on the Pacific coast of Japan. We find that the dominant period of this tsunami was relatively short, 250 sec, and that the largest tsunami occurred at 21:13 (6:13 JST) near Sofu-gan volcano. In addition, T waves, or the ocean-acoustic waves, were clearly observed by DONET – we posit these correspond to a vigorous swarm-like seismic event at the same region of the tsunami source. We formally invert for the tsunami source and find that several tsunami sources with an interval of about 4 min are necessary to reproduce the observed records. These most likely correspond to volcanic eruptions.

概要   2023 年 10 月 9 日 (JST) に鳥島近海において発生した津波について、日本列島太平洋沖に展開されている DONET および S-net の水圧計記録を解析した。その結果、(1) 約 250 秒の短周期成分が卓越した津波だったこと、(2) 最大波は 6 時 13 分 (JST) に発生したことが明らかとなった。また最大波について津波インバージョンを用いて波源推定を行ったところ、媀婦岩西側の領域に波源が求まった。また、6 時 13 分から 4 分間隔で計 3 回の津波の発生を仮定したモデルが、単一の津波生成を仮定したモデルに比べて観測記録をよく説明した。

1. Introduction

On October 8, 2023, at 21:40 UTC (6:40 on October 9 in Japan Standard Time; JST), the Japan Meteorological Agency (JMA) issued a tsunami warning for the Izu Islands, and for the Pacific coast of Japan from Chiba Prefecture to Kagoshima Prefecture (Figure 1a). The warning was issued after observing anomalous increases in water levels at the tide gauge at the Izu Islands. The largest tsunami was observed at Hachijo-jima Island (60 cm) and 10-40 cm tsunamis were observed over southwest Japan (Japan Meteorological Agency, 2023). This tsunami was at first thought to be caused by an earthquake 75 mins before the warning, at 20:25 UTC (5:25 JST), whose moment magnitude (M_w) was 4.7 as estimated by the United States Geological Survey (USGS). Events of this magnitude typically have coseismic deformation < 1 cm, which is far too small to cause hazardous tsunamis. This suggests that the tsunami might not have been associated with the earthquake and was possibly caused by a non-seismic source.

Today real-time ocean-bottom observation networks, called DONET and S-net, have been deployed on the Pacific coast of Japan and their ocean-bottom pressure

(OBP) records have been used for tsunami analyses (e.g., Aoi et al., 2020, Figures 1a and S1). Because of their dense and widespread deployment, we can easily detect small tsunami signals and identify their origin by computing the theoretical tsunami travel times from candidate sources to stations. In this paper, we first detect the tsunami signal from these OBP records, identify their potential origin from travel times and then formally estimate a tsunami source model of this event.

2. Data

We downloaded the 10 Hz sampled OBP records of DONET and S-net from the website of the National Research Institute for Earth Science and Disaster Resilience (NIED; https://www.seafloor.bosai.go.jp/). The time window used in this study was 4 hours between 20:00 and 24:00 UTC (from 5:00 to 9:00 JST). DONET and S-net have sub-networks named DONET1 and DONET2, and S1, S2, S3, S4, S5, and S6, respectively; each consisting of 22 to 29 sensors. For DONET1 and DONET2 there was little characteristic difference in the records of this event, so we will refer to them collectively as DONET in this paper. For preprocessing, we fitted the cubic functions to raw OBP data and removed the long-period components such as the ocean tide and the DC or static com-
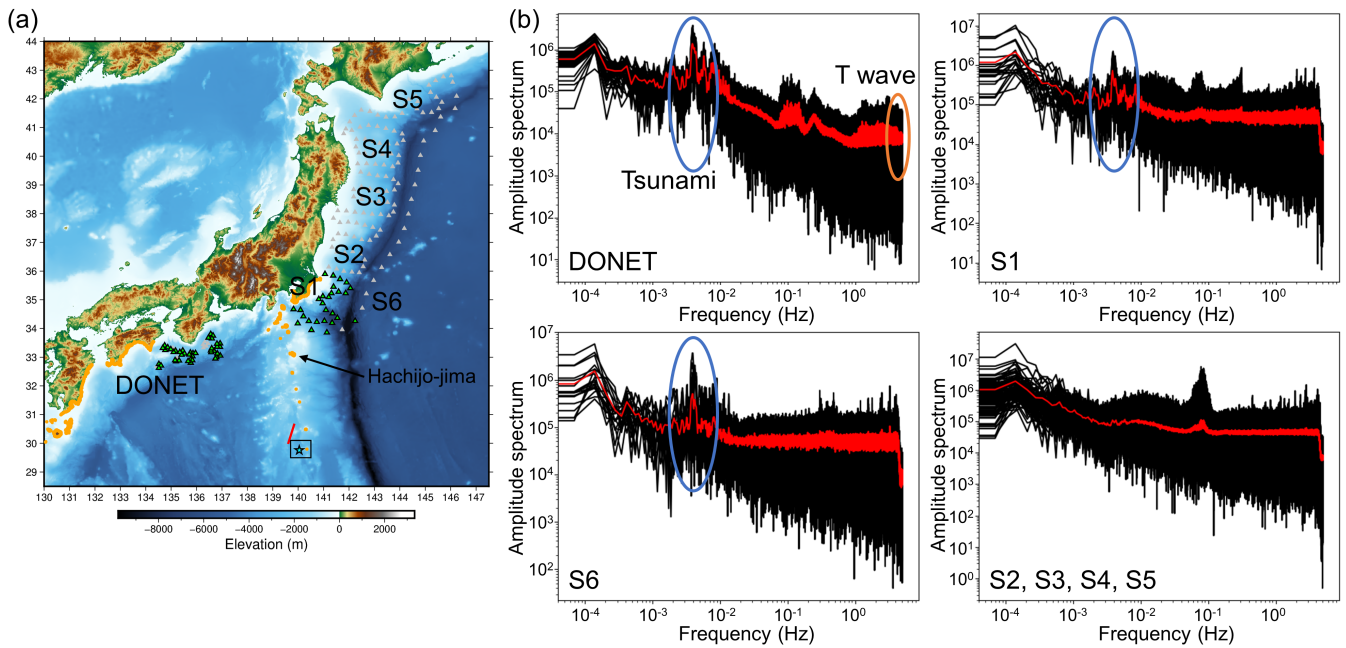
Figure 1 (a) Station distribution of DONET and S-net. The green triangles are the stations used for the tsunami source modeling; the grays are existing sites not used in the modeling. The orange lines show the area where the tsunami warning was issued by the JMA. The cyan star represents the source for the travel time calculation, i.e., the average location of the swarm-like seismic event. The black rectangle is the area of Figure 3. The red line represents the location of the pumice raft observed by the Japan Coast Guard on October 20. The elevation data comes from ETOPO1. (b) Amplitude spectrum of DONET and S-net OBP records. The black lines are the spectrum of each station, and the red ones are their average.

ponent due to the station depth.

3. Tsunami Detection

To establish whether individual records show evidence of the tsunami, first we investigated them in the frequency domain. Figure 1b shows the amplitude spectrum of DONET, S1, S6, and the other subnetworks calculated using the Fast Fourier Transform with the Tukey window. The stations in DONET, S1, and S6 clearly observed a signal with a dominant period of ~250 sec (~0.004 Hz), which is much less clear in the other S-net stations. In subnetwork S6, only southern stations observed such tsunamis (Figure S2). That is most likely because of the refraction at the Japan Trench and the Izu-Bonin Trench which acts as a waveguide and focuses energy towards southwest Japan (e.g., Heidarzadeh and Satake, 2014). In addition, only DONET stations observed the high-frequency signal (>2 Hz). Though there is also a small peak at around 10 sec (0.1 Hz), we do not treat it in this study because this frequency range is known to be associated with the sea ground acceleration (Kubota et al., 2020; Mizutani et al., 2020; Nosov et al., 2018).

To establish the detection of the above signals in the time domain, we calculated theoretical tsunami and acoustic wave travel times from the source to the stations. The M_w 4.7 earthquake occurred at 20:25 UTC as one of the events of a longer-lived swarm-like event; in fact, 14 earthquakes were detected by the USGS from 19:53 to 21:26 UTC. We therefore initially set the potential source locations for travel time calculation to the average of these earthquake locations (140.04°E, 29.76°N; Figure 1a).

We used the Fast Marching Method (FMM) to calculate the theoretical travel times (Sethian, 1999). The phase speed maps for the FMM were calculated with the 0.02° gridded bathymetry based on the ETOPO1 (Amante and Eakins, 2009) for the tsunami, and as the constant value of 1500 m/s for the T wave. Since the dispersive effect cannot be ignored for the tsunami with the dominant period of 250 sec, the tsunami phase speed map was calculated accounting for the dispersion using the method of Sandanbata et al. (2017).

Figure 2a shows the tsunami waveforms at DONET stations, which were time-shifted by the theoretical travel time from (140.04°E, 29.76°N). Here, we set the origin of lapse time to 20:25 UTC (5:25 JST), that is, if the tsunami waves had been generated at that source location at 20:25 UTC, they would align at $t = 0$. Any delay forward or backward in time indicates either that the origin time or the source location is incorrect. To focus on the tsunami and high-frequency signals, we applied the band-pass filters of 100–1000 sec and 1–4 Hz to the OBP records (Figures 2a and 2c).

In the tsunami records (Figure 2a), we can see clear coherent signals. The largest tsunami is observed approximately 2900 sec after the origin time and continues for 1500 sec (the period between two vertical red lines; Figure 2b). Since we shifted the OBP records with the tsunami travel time, it indicates that the largest tsunami occurred not at 20:25 UTC (5:25 JST) but most likely ~48 mins later at 21:13 UTC (6:13 JST). At that time, another earthquake with M_b 5 according to the USGS earthquake catalog (black dashed line in Figure 2 and Table S1). It is also possible that the time shift is due to the source location being wrong, however if that were the case
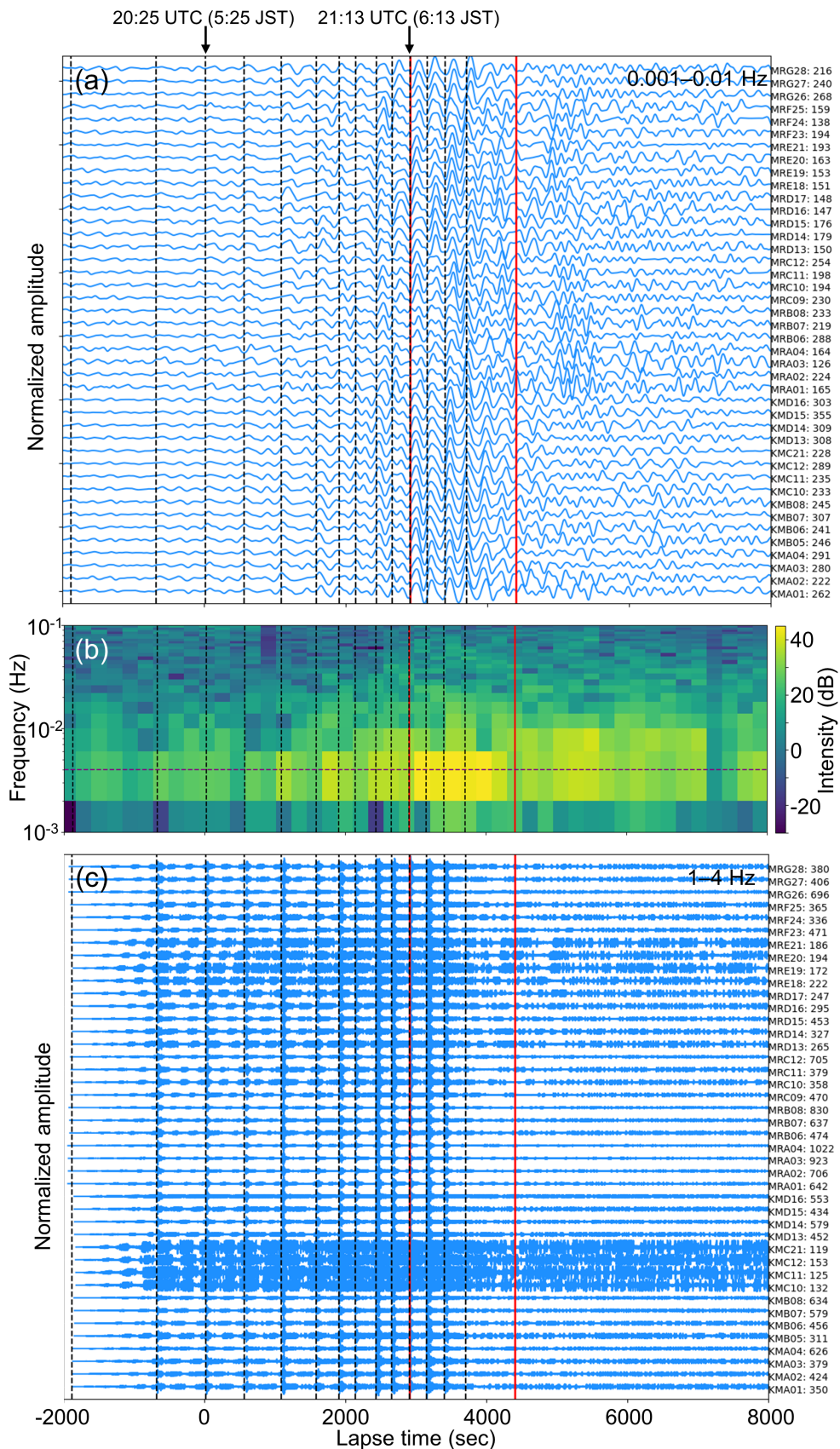
Figure 2 (a) Time-shifted OBP records of DONET with the theoretical travel time of tsunami and the band-pass filter of 100 – 1000 sec. Each record is normalized to the maximum amplitude, which is described with the station name on the right (unit is Pa). The black dashed lines are the origin time of the earthquakes detected by the USGS. The red vertical lines represent the time window used in the tsunami waveform inversion. (b) Spectrogram at station KMA01. The horizontal axis and the vertical lines are the same as (a). The horizontal purple line represents the frequency of 0.004 Hz. (c) Same as (a) except that the T wave, that is, the time-shifted records with the T wave travel time and the band-pass filter of 1 – 4 Hz.

the waveforms would not be coherent and would show a "move out" or distance-dependent time shift which is not seen in the record section. In other words, the tsunami was associated somehow with the swarm-like event in the Izu Islands, but its main wave was generated at 21:13 UTC (6:13 JST).

In the high-frequency OBP records (Figure 2c), we can find several waves corresponding to the earthquakes in the USGS catalog (black dashed lines). Since we shifted these records with the travel time of the ocean acoustic wave, these can be considered as the T wave. The signal to noise ratio at stations KMC10, KMC11, KMC12, KMC21, MRD17, MRE18, MER19, MER20, and MRE21 were worse than the others. This is because the deployment depth of these stations is deeper than 2500 m, which is deeper than the SOFAR channel, which typically exists at around 1200 m, where the T wave is trapped. Because there are the Izu Islands between the source and S-net, the T wave was observed only at DONET (Fig 1).

4. Tsunami Source Estimation

Having established that the tsunami likely originates from the area around an active swarm, in this section, we estimate the tsunami source model (the initial sea-surface disturbance) by tsunami waveform inversion. From the result in Section 3, we assumed that the tsunami occurred at 21:13 UTC, and set the target area to cover the swarm-like seismic event: from 139.81°E to 140.37°E in the east-west direction; and from 29.56°N to 29.96°N in the north-south direction. We estimated the sea surface displacement with the following equation:

$$\begin{bmatrix} d \\ 0 \end{bmatrix} = \begin{bmatrix} G \\ \alpha S \end{bmatrix} m$$

where d, G, S and m are the data vector, kernel matrix (Green's functions), spatial smoothing matrix, and model vector, respectively. We solved this equation by the singular value decomposition. The weight parameter α and threshold of the singular value are determined based on the trade-off curve of the variance reduction (VR) and model variance. In this study, the variance reduction is defined as:

$$VR = \left(1 - \frac{\sum_i \int \left[u_i^{OBS}(t) - u_i^{SYN}(t) \right]^2 dt}{\sum_i \int \left[u_i^{OBS}(t) \right]^2 dt} \right) \times 100[\%]$$

where $u_i^{OBS}(t)$ and $u_i^{SYN}(t)$ are the observed and synthetic waveforms at station i. For calculating the kernel matrix or Green's functions, we used JAGURS (Baba et al., 2015; Saito et al., 2010), the open-source tsunami calculation code, and made synthetic tsunami records considering the dispersive effect. For the bathymetry data, the same as in the travel time estimation was used. Potential sources were represented as the 2D Gaussian function with an amplitude of 1 m, a width (i.e., variance) of 4 km, and set on a regular grid each 0.04° in latitude and longitude. We used the records of DONET, and S1 and S6 subnetworks of S-net, which are shown

as green triangles in Figure 1a. The records were pre-processed and applied the band-pass filter of 100–1000 sec as same as in the previous section. The time window for the inversion analysis was 1500 sec from the theoretical travel time, represented as red vertical lines in Figure 2.

Sandanbata et al. (2023) estimated the tsunami source time function using the records of DONET1 and suggested that several tsunamigenic events, some of which occurred at the same time as the T wave events, can explain the observed record. Since two additional earthquakes with T waves were observed after 21:13 UTC, at 21:17 and 21:21 UTC, we conducted a multiple time window inversion (Hossen et al., 2015; Satake et al., 2013) to consider these events by which we allow tsunami sources at these three different times to contribute to the inversion. In other words, three kinds of Green's functions, the second and third ones were shifted in time of 4 min and 8 min from the first one, were involved in the kernel matrix. Note that each synthetic tsunami was assumed to occur instantaneously.

Figure 3 shows the tsunami source model. We chose the model with the smoothing parameter of 0.1 and the threshold of the singular value of 0.2 as the best model, whose VR was 64.1% (Figure S3). At all the time steps, the large uplift (>0.2 m) was located to the northeast of the swarm-like event. The uplift at 21:17 UTC was slightly smaller than the others. In addition, at 21:21 UTC, there was a subsidence of 0.27 m in the east of the target area.

5. Discussion

To investigate the uncertainty of our tsunami source model, we employed a bootstrap approach with 100 sample inversions (Chernick, 2007). We randomly selected OBP stations for each inversion process and calculated the average and standard deviation of the results. The estimated standard deviation is less than 0.06 m (Figure S4), sufficiently small compared to the source amplitude. In addition, the inversion result with other smoothing and damping parameters was confirmed (Figure S5). In all the cases, the large uplift (>0.2 m) on the northeast of the earthquake swarm is stably estimated. On the other hand, the subsidence peak on the east of the uplift is varied with parameter selection. We therefore conclude that the main source of this tsunami event is the uplift on the northeast of the seismic swarm.

In the previous section, we conducted the multiple time window inversion based on the observed T wave signals. To confirm the effectiveness of using the multiple time window, we conducted the same inversion except for the single tsunami source at 21:13 UTC (Figure S6). As a result, although we obtained the same pattern as in Figure 3a, the VR became worse (43.0%). In other words, the multiple tsunami source is more appropriate than the single source for this tsunami event. At 21:26 or after the three tsunamigenic events considered so far, another earthquake without T wave (M_b 4.5) was detected by the USGS (Fig 2c and Table S1). We conducted the multiple time window inversion including this event
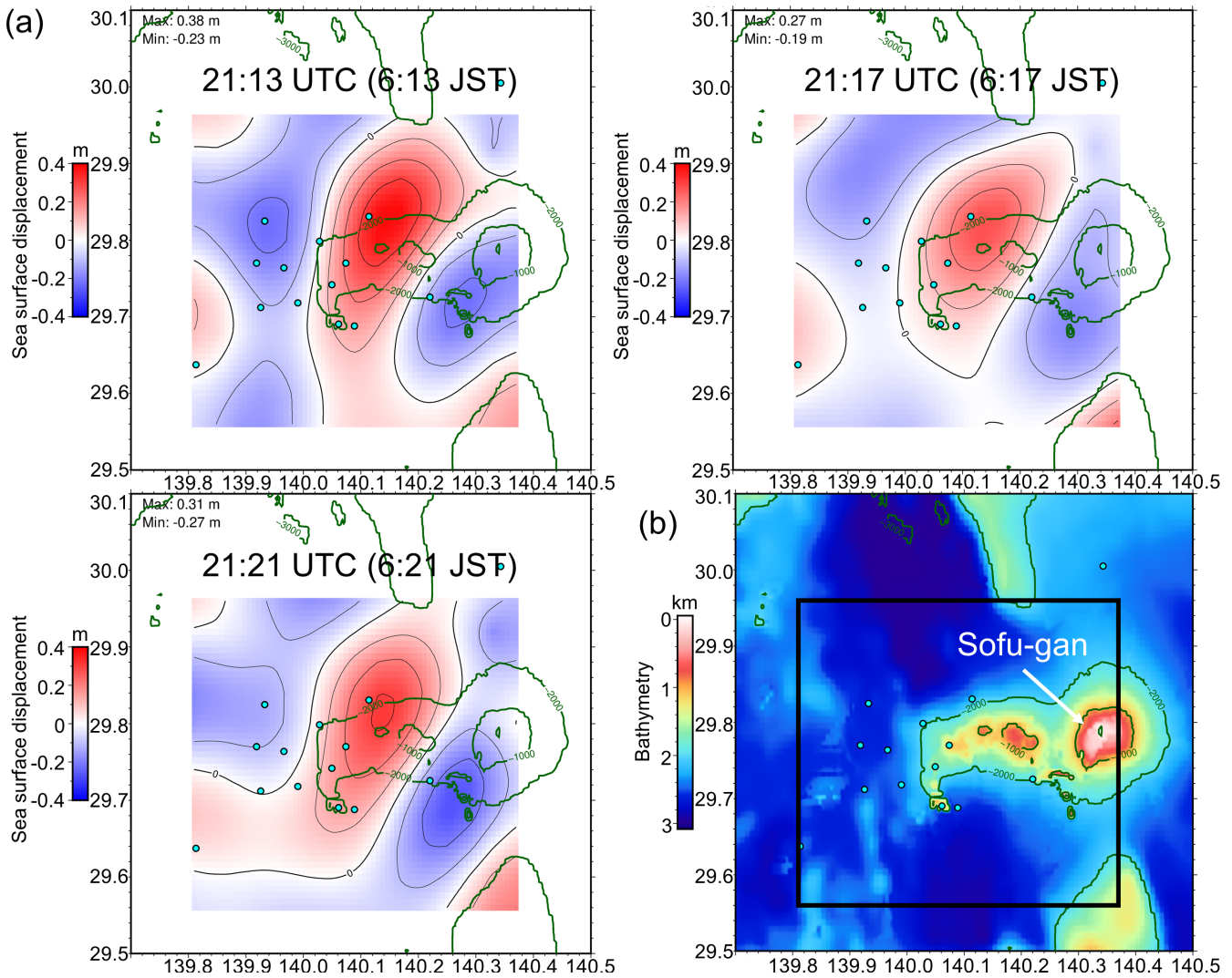
Figure 3 (a) Tsunami source models at 21:13, 21:17, and 21:21 UTC with the contours at each 0.1 m. The cyan circles represent the epicenter distribution of the earthquakes detected by the USGS. The green contours are the bathymetry at each 1000 m. (b) Bathymetry map at the area of (a). The black rectangle is the target area of the tsunami inversion analysis.

(i.e., four tsunami sources; Figure S7), but the VR increased little (65.9%; the improvement is 1.8%). We therefore conclude that the earthquake at 21:26 did not contribute to the observed tsunami, i.e., three seismic events with T wave are the main source of this tsunami.

Figure S8 compares the observed records with the synthetic ones calculated from the inversion results. Even when considering the multiple tsunami sources, the synthetic records have a smaller amplitude than the observed ones. This may be because we considered the tsunami events only after 21:13, i.e., our model cannot explain the later phase of tsunamis that occurred before 21:13.

It is interesting that the time interval of T wave generation (4 min) agrees with the dominant period of the tsunami (250 sec). Although more investigations are necessary, the occurrence interval of the earthquakes might enhance the 250-sec period tsunami (Sandanbata et al., 2023).

As discussed above, the tsunami was generated on the northeast of the swarm-like event of the earthquake. Immediately due east of the swarm, there is an active volcano named Sofu-gan (Figure 3b; Geological Survey of Japan, 2013). The uplifts at all time steps of the estimated tsunami source are adjacent to the western bulge of the Sofu-gan volcano. Based on this result, we speculate that the tsunami and seismic swarm were caused by the intermittent volcanic eruptions, whose vent opened on the western bulge of the Sofu-gan volcano and generated the sea surface uplift; and the eruption ended at 21:21 UTC. It is consistent with that the earthquakes that generated T waves stopped at 21:21 UTC (Figure 2c). In addition, although the exact details of the source are unknown, on October 20, 11 days after this event, a pumice raft with a length of 80 km was observed northwest of the Sofu-gan volcano by the Japan Coast Guard (Japan Coast Gard, 2023). The last recorded eruption of the Sofu-gan volcano was in 1975 (Geological Survey of Japan, 2013). The tsunami and swarm-like seismic event analyzed in this paper may be possibly associated with the new eruption.

6. Conclusions

Based on the OBP records of DONET and S-net, we revealed that the tsunami on October 8 (October 9 JST) was

a short-period tsunami with a dominant period of 250 sec. The origin time of the largest tsunami was 21:13 UTC (6:13 JST). We also estimated the tsunami source model. It suggested that multiple tsunami sources are necessary to reproduce the observed records. This paper focused only on the largest tsunami that occurred at 21:13 UTC. In Figure 2a, however, there are other coherent signals outside of the time window for the source estimation. Constructing the source model based on the whole tsunami records will help to understand the details of this event.

Acknowledgements

Data and code availability

The OBP records of DONET (National Research Institute for Earth Science and Disaster Resilience (NIED), 2019b) and S-net (National Research Institute for Earth Science and Disaster Resilience (NIED), 2019a) can be downloaded from the NIED website (https://www.seafloor.bosai.go.jp/, in Japanese) with data request and permission. The USGS earthquake catalog can be accessed from the USGS website (https://earthquake.usgs.gov/earthquakes/search/). The JAGURS code calculating synthetic tsunamis is freely available from GitHub (https://github.com/jagurs-admin/jagurs). Some figures were made by the Generic Mapping Tools (GMT; Wessel et al., 2019). To plot the tsunami warning area, the data from the ROIS-DS Center for Open Data in the Humanities (https://geoshape.ex.nii.ac.jp/jma/resource/AreaTsunami/) was used.

Competing interests

The authors have no competing interests.

References

Amante, C. and Eakins, B. *ETOPO1 Global Relief Model converted to PanMap layer format*. PANGAEA, 2009. doi: 10.1594/PANGAEA.769615.

Aoi, S., Asano, Y., Kunugi, T., Kimura, T., Uehira, K., Takahashi, N., Ueda, H., Shiomi, K., Matsumoto, T., and Fujiwara, H. MOWLAS: NIED observation network for earthquake, tsunami and volcano. *Earth, Planets and Space*, 72(1), Sept. 2020. doi: 10.1186/s40623-020-01250-x.

Baba, T., Takahashi, N., Kaneda, Y., Ando, K., Matsuoka, D., and Kato, T. Parallel Implementation of Dispersive Tsunami Wave Modeling with a Nesting Algorithm for the 2011 Tohoku Tsunami. *Pure and Applied Geophysics*, 172(12):3455 – 3472, Feb. 2015. doi: 10.1007/s00024-015-1049-2.

Chernick, M. R. *Bootstrap Methods: A Guide for Practitioners and Researchers*. Wiley, Apr. 2007. doi: 10.1002/9780470192573.

Geological Survey of Japan. *Sofugan, Volcano of Japan*. 2013. https://gbank.gsj.jp/volcano/Quat_Vol/volcano_data/G19.html.

Heidarzadeh, M. and Satake, K. The El Salvador and Philippines Tsunamis of August 2012: Insights from Sea Level Data Analysis and Numerical Modeling. *Pure and Applied Geophysics*, 171(12): 3437 – 3455, Feb. 2014. doi: 10.1007/s00024-014-0790-2.

Hossen, M. J., Cummins, P. R., Dettmer, J., and Baba, T. Tsunami waveform inversion for sea surface displacement following the 2011 Tohoku earthquake: Importance of dispersion and source kinematics. *Journal of Geophysical Research: Solid Earth*, 120 (9):6452 – 6473, Sept. 2015. doi: 10.1002/2015jb011942.

Japan Coast Gard. Press release about suspended solids in the sea around Torishima Island, 2023. https://www.kaiho.mlit.go.jp/info/kouhou/r5/k231020_1/k231020_1.pdf. Observed on October 20.

Japan Meteorological Agency. Press release about the earthquake near Tori-shima Island at 05:25 on October 9, 2023. 2023. https://www.jma.go.jp/jma/press/2310/09b/kaisetsu202310091100.pdf.

Kubota, T., Saito, T., Chikasada, N. Y., and Suzuki, W. Ultrabroadband Seismic and Tsunami Wave Observation of High-Sampling Ocean-Bottom Pressure Gauge Covering Periods From Seconds to Hours. *Earth and Space Science*, 7(10), Sept. 2020. doi: 10.1029/2020ea001197.

Mizutani, A., Yomogida, K., and Tanioka, Y. Early Tsunami Detection With Near-Fault Ocean-Bottom Pressure Gauge Records Based on the Comparison With Seismic Data. *Journal of Geophysical Research: Oceans*, 125(9), Aug. 2020. doi: 10.1029/2020jc016275.

National Research Institute for Earth Science and Disaster Resilience (NIED). *NIED S-net*. 2019a. doi: 10.17598/nied.0007.

National Research Institute for Earth Science and Disaster Resilience (NIED). *NIED DONET*. 2019b. doi: 10.17598/nied.0008.

Nosov, M., Karpov, V., Kolesov, S., Sementsov, K., Matsumoto, H., and Kaneda, Y. Relationship between pressure variations at the ocean bottom and the acceleration of its motion during a submarine earthquake. *Earth, Planets and Space*, 70(1), June 2018. doi: 10.1186/s40623-018-0874-9.

Saito, T., Satake, K., and Furumura, T. Tsunami waveform inversion including dispersive waves: the 2004 earthquake off Kii Peninsula, Japan. *Journal of Geophysical Research: Solid Earth*, 115 (B6), June 2010. doi: 10.1029/2009jb006884.

Sandanbata, O., Watada, S., Satake, K., Fukao, Y., Sugioka, H., Ito, A., and Shiobara, H. Ray Tracing for Dispersive Tsunamis and Source Amplitude Estimation Based on Green's Law: Application to the 2015 Volcanic Tsunami Earthquake Near Torishima, South of Japan. *Pure and Applied Geophysics*, 175(4):1371 – 1385, Dec. 2017. doi: 10.1007/s00024-017-1746-0.

Sandanbata, O., Satake, K., Takemura, S., Watada, S., and Maeda, T. Enigmatic tsunami waves amplified by repetitive source events in the southwest of Torishima Island, Japan. *Not peer-reviewed preprint, ESS Open Archive*, Oct. 2023. doi: 10.22541/essoar.169878726.62136311/v1.

Satake, K., Fujii, Y., Harada, T., and Namegaya, Y. Time and Space Distribution of Coseismic Slip of the 2011 Tohoku Earthquake as Inferred from Tsunami Waveform Data. *Bulletin of the Seismological Society of America*, 103(2B):1473 – 1492, May 2013. doi: 10.1785/0120120122.

Sethian, J. *Level Set Methods and Fast Marching Methods*. Cambridge Unversity Press, 2nd edition, 1999.

Wessel, P., Luis, J. F., Uieda, L., Scharroo, R., Wobbe, F., Smith, W. H. F., and Tian, D. The Generic Mapping Tools Version 6.